

Bayesian inference of the symmetry energy and the neutron skin in ^{48}Ca and ^{208}Pb from CREX and PREX-2

Zhen Zhang^{1,*} and Lie-Wen Chen^{2,†}

¹*Sino-French Institute of Nuclear Engineering and Technology, Sun Yat-sen University, Zhuhai 519082, China*

²*School of Physics and Astronomy, Shanghai Key Laboratory for Particle Physics and Cosmology, and Key Laboratory for Particle Astrophysics and Cosmology (MOE), Shanghai Jiao Tong University, Shanghai 200240, China*



(Received 18 July 2022; revised 2 August 2023; accepted 11 August 2023; published 21 August 2023)

Using the recent model-independent determination of the charge-weak form factor difference ΔF_{CW} in ^{48}Ca and ^{208}Pb by the CREX and PREX-2 collaborations together with some well-determined properties of doubly magic nuclei, we perform Bayesian inference of the symmetry energy $E_{\text{sym}}(\rho)$ and the neutron skin thickness Δr_{np} of ^{48}Ca and ^{208}Pb within the Skyrme energy density functional (EDF). We find the inferred $E_{\text{sym}}(\rho)$ and Δr_{np} separately from CREX and PREX-2 are compatible with each other at 90% C.L., although they are inconsistent at 68.3% C.L. with CREX (PREX-2) favoring a very soft (stiff) $E_{\text{sym}}(\rho)$ and rather small (large) Δr_{np} . By combining the CREX and PREX-2 data, we obtain a soft symmetry energy around saturation density ρ_0 and thinner Δr_{np} of ^{48}Ca and ^{208}Pb , which are found to be closer to the corresponding results from CREX alone, implying the PREX-2 is less effective to constrain the $E_{\text{sym}}(\rho)$ and Δr_{np} due to its lower precision of ΔF_{CW} . Furthermore, we find the Skyrme EDF results inferred by combining the CREX and PREX-2 data nicely agree with the measured dipole polarizabilities α_D in ^{48}Ca and ^{208}Pb as well as the neutron matter equation of state from microscopic calculations. The implications of the inferred soft $E_{\text{sym}}(\rho)$ around ρ_0 are discussed.

DOI: [10.1103/PhysRevC.108.024317](https://doi.org/10.1103/PhysRevC.108.024317)

I. INTRODUCTION

The CREX [1] and PREX-2 [2] Collaborations recently reported the model-independent extractions of the difference between the charge form factor F_C and the weak form factor F_W , i.e., $\Delta F_{\text{CW}}(q) \equiv F_C(q) - F_W(q) = 0.0277 \pm 0.0055$ at $q = 0.8733 \text{ fm}^{-1}$ for ^{48}Ca and $\Delta F_{\text{CW}}(q) = 0.041 \pm 0.013$ at a smaller four-momentum transfer $q = 0.3977 \text{ fm}^{-1}$ for ^{208}Pb [1]. Since these extractions are free from the strong interaction uncertainties, they allow us to determine with minimal model dependence the neutron skin thickness $\Delta r_{\text{np}} \equiv r_n - r_p$ [$r_n(\rho)$ is the neutron (proton) rms radius of the nucleus] and further to constrain the density dependence of the symmetry energy $E_{\text{sym}}(\rho)$ [3–12]. The $E_{\text{sym}}(\rho)$ encodes the isospin dependence of nuclear matter equation of state (EOS) and plays an important role in both nuclear physics and astrophysics [13–16].

From the PREX-2 data, the Δr_{np} of ^{208}Pb is extracted to be $0.283 \pm 0.071 \text{ fm}$ [2]. An analysis based on a relativistic energy density functional (EDF) indicates the PREX-2 data leads to a very stiff $E_{\text{sym}}(\rho)$ with a rather large symmetry energy slope parameter [$L(\rho_r) = 3\rho_r \frac{dE_{\text{sym}}(\rho)}{d\rho}|_{\rho_r}$] of $L \equiv L(\rho_0) = 106 \pm 37 \text{ MeV}$ at saturation density ρ_0 [17], which challenges our present understanding on the $E_{\text{sym}}(\rho)$ [18–20]. Many studies have been devoted to understanding the PREX-2 result and its implications in nuclear physics and astrophysics

[17,21–24]. In particular, the tension between the PREX-2 data and the measured electric dipole polarizabilities α_D in ^{48}Ca and ^{208}Pb at RCNP in Osaka [25–27] is observed with the latter favoring a much softer $E_{\text{sym}}(\rho)$ [22,23].

Very remarkably, the CREX adopts the same experimental approach as PREX-2 and recently reports a rather thin neutron skin of $\Delta r_{\text{np}} = 0.121 \pm 0.026(\text{exp}) \pm 0.024(\text{model}) \text{ fm}$ in ^{48}Ca [1]. Analyses with a number of modern nonrelativistic and relativistic EDFs [28,29] (see also Ref. [1]) suggest a significant tension between the CREX and PREX-2 results, calling for further critical theoretical and experimental investigations.

In this work, we employ the Bayesian inference method, which provides a consistent probabilistic approach to extract quantitative information from experimental data [30], to analyze the CREX and PREX results on the $\Delta F_{\text{CW}}(q)$ together with other well-known data of eight doubly magic nuclei, i.e., ^{16}O , ^{40}Ca , ^{48}Ca , ^{56}Ni , ^{68}Ni , ^{100}Sn , ^{132}Sn , and ^{208}Pb , based on the Skyrme EDF. We show the CREX and PREX-2 results are compatible at 90% confidence level (C.L.), although they are inconsistent with each other at 68.3% C.L., and furthermore the PREX-2 is less effective to constrain the $E_{\text{sym}}(\rho)$ and Δr_{np} due to its lower precision of ΔF_{CW} compared to the CREX. By combining the CREX and PREX-2 results at 90% C.L., we find a soft $E_{\text{sym}}(\rho)$ around ρ_0 can be inferred and the Skyrme EDF can nicely describe the measured α_D in ^{48}Ca and ^{208}Pb as well as the neutron matter EOS from microscopic many-body calculations.

*Corresponding author: zhangzh275@mail.sysu.edu.cn

†Corresponding author: lwchen@sjtu.edu.cn

TABLE I. Prior ranges of the ten parameters used, together with the posterior median values and 68.3% (90%) credible intervals from B-All and the parameter values of the Skyrme interaction SkREx.

Quantity	prior	posterior (B-All)	SkREx
ρ_0 (fm ⁻³)	[0.155, 0.165]	0.1619 ^{+0.0015(0.0023)} _{-0.0016(0.0026)}	0.1618
E_0 (MeV)	[-16.5, -15.5]	-16.002 ^{+0.063(0.100)} _{-0.063(0.103)}	-16.00
K_0 (MeV)	[210, 250]	225.0 ^{+2.9(4.9)} _{-2.8(4.6)}	223.1
$E_{\text{sym}}(\rho_0)$ (MeV)	[22, 55]	29.1 ^{+2.1(3.6)} _{-1.8(2.7)}	29.2
L (MeV)	[-90, 240]	17.1 ^{+23.8(39.3)} _{-22.3(36.0)}	13.0
G_S (MeV · fm ⁵)	[110, 170]	117.9 ^{+6.4(11.8)} _{-4.2(6.2)}	118.9
G_V (MeV · fm ⁵)	[-70, 70]	-27.3 ^{+46.5(73.6)} _{-31.0(39.1)}	-55.0
W_0 (MeV · fm ⁵)	[90, 140]	105.4 ^{+5.0(8.3)} _{-4.9(7.9)}	117.2
$m_{s,0}^*/m$	[0.7, 1.0]	0.95 ^{+0.03(0.04)} _{-0.06(0.10)}	0.969
$m_{v,0}^*/m$	[0.6, 0.9]	0.71 ^{+0.11(0.16)} _{-0.08(0.10)}	0.640

II. MODEL AND METHOD

The nuclear properties are calculated within the widely used standard Skyrme EDF. Since we focus on doubly magic nuclei, pairing interaction is not taken into account. The Skyrme EDF can then be characterized by ten parameters: the ρ_0 , the binding energy per nucleon of symmetric nuclear matter $E_0(\rho_0)$, the incompressibility K_0 , $E_{\text{sym}}(\rho_0)$, L , the isoscalar effective mass $m_{s,0}^*$ and the isovector effective mass $m_{v,0}^*$ at ρ_0 , the gradient coefficient G_S , the symmetry-gradient coefficient G_V , and the spin-orbit coupling constant W_0 [31–33]. Based on the Skyrme EDF, once given a parameter set

$$\mathbf{p} = \{\rho_0, E_0(\rho_0), K_0, E_{\text{sym}}(\rho_0), L, G_S, G_V, W_0, m_{s,0}^*, m_{v,0}^*\}, \quad (1)$$

the ground-state properties of finite nuclei are calculated with the Hartree-Fock (HF) method, and the breathing mode energy is obtained from the constrained HF (CHF) calculation.

The calibration and uncertainty quantification of the ten parameters is carried out using a Bayesian approach. According to Bayes' theorem, the posterior distribution of model parameters \mathbf{p} , given experimental data \mathcal{O}^{exp} for a set of observables \mathcal{O} , can be evaluated as

$$P(\mathbf{p} | \mathcal{M}, \mathcal{O}^{\text{exp}}) = \frac{P(\mathcal{O}^{\text{exp}} | \mathcal{M}, \mathbf{p})P(\mathbf{p})}{\int P(\mathcal{O}^{\text{exp}} | \mathcal{M}, \mathbf{p})P(\mathbf{p})d\mathbf{p}}, \quad (2)$$

where \mathcal{M} is the given model, $P(\mathbf{p})$ is the prior probability density of model parameters \mathbf{p} before being confronted with the data \mathcal{O}^{exp} , and $P(\mathcal{O}^{\text{exp}} | \mathcal{M}, \mathbf{p})$ denotes the likelihood of observing \mathcal{O}^{exp} with given model \mathcal{M} predictions at \mathbf{p} . The prior distribution of \mathbf{p} are normally chosen to be uniform in their empirical ranges listed in Table I. In particular, given the rather thick (thin) neutron skin in ²⁰⁸Pb (⁴⁸Ca) from PREX-2 (CREX), the prior ranges of $E_{\text{sym}}(\rho_0)$ and L are taken to be as large as 22 to 55 MeV and -90 to 240 MeV, respectively, to avoid the prior range dependence of the posterior results.

The likelihood function is taken to be the commonly used Gaussian form

$$P(\mathcal{M}, \mathcal{O}_i^{\text{exp}} | \mathbf{p}) \propto \exp \left\{ - \sum_i \frac{[\mathcal{O}_i(\mathbf{p}) - \mathcal{O}_i^{\text{exp}}]^2}{2\sigma_i^2} \right\}, \quad (3)$$

where $\mathcal{O}_i(\mathbf{p})$ is the model prediction on the i th observable for a given parameter set \mathbf{p} , $\mathcal{O}_i^{\text{exp}}$ is the corresponding data, and σ_i is the adopted error.

To estimate the posterior distribution given by Eq. (2), the Markov chain Monte Carlo (MCMC) process is carried out using the Metropolis-Hasting algorithm. We first run 5×10^5 burn-in MCMC steps to allow the chain to reach equilibrium, and then generate 10^6 MCMC steps in parameter space. The posterior distributions of model parameters and observables are estimated from 15 parallel MCMC process, i.e., 1.5×10^7 MCMC samples.

III. SELECTED OBSERVABLES

The key observables in this work are the model-independent ΔF_{CW} in ⁴⁸Ca and ²⁰⁸Pb, i.e., $\Delta F_{\text{CW}}^{48} \equiv \Delta F_{\text{CW}}(q = 0.8733 \text{ fm}^{-1})$ from CREX [1] and $\Delta F_{\text{CW}}^{208} \equiv \Delta F_{\text{CW}}(q = 0.3977 \text{ fm}^{-1})$ from PREX-2 [2]. The normalized nuclear form factors $F_C(q)$ and $F_W(q)$ are calculated by folding the nucleon form factor $F_t(q)$ ($t = n, p$) and the spin-orbit current form factor (F_t^{ls}) with the intrinsic nucleon electromagnetic form factor $G_{E/M,t}$ and weak form factor $G_{E/M,t}^{(W)}$ by [23]

$$F_C(q) = \frac{1}{Z} \sum_{t=p,n} [G_{E,t}(q)F_t(q) + G_{M,t}(q)F_t^{(ls)}(q)], \quad (4)$$

$$F_W(q) = \sum_{t=p,n} \frac{[G_{E,t}^{(W)}(q)F_t(q) + G_{M,t}^{(W)}(q)F_t^{(ls)}(q)]}{ZQ_p^{(W)} + NQ_n^{(W)}}, \quad (5)$$

where $N(Z)$ is the neutron(proton) number, and $Q_p^{(W)} = 0.0713$ and $Q_n^{(W)} = -0.9888$ are proton and neutron weak charges, respectively. The $G_{E/M,t}$ are derived from the isospin-coupled Sachs form factors, the relativistic Darwin correction has been included and the center-of-mass corrections are taken into account by simply renormalizing the nucleon mass m_N to $(1 - 1/A)m_N$ in the HF calculation (see, e.g., Ref. [34] for details). From $G_{E/M,t}$, the $G_{E/M,t}^{(W)}$ can then be determined by further considering the contribution of the strange-quark electromagnetic form factors $G_{E/M,s}$ (see, Ref. [23] for details). In addition, the $F_C(q)$ at low momentum q can be characterized by three parameters [35], i.e., the charge rms radius

$$r_c = \sqrt{-\frac{3}{F_C(0)} \frac{d^2 F_C(q)}{dq^2} \Big|_{q=0}}, \quad (6)$$

the diffraction radius $R_d = \frac{4.493}{q_0}$ determined from the first zero of $F_C[q_0] = 0$, and the surface thickness

$$\sigma = \sqrt{\frac{2}{q_m} \log \left[\frac{3j_1(q_m R_d)}{q_m R_d F_C(q_m)} \right]}, \quad q_m = 5.6/R, \quad (7)$$

where $j_1(x) = \frac{\sin x}{x^2} - \frac{\cos x}{x}$ is the spherical Bessel function of the first kind.

TABLE II. Experimental data and adopted errors used in the Bayesian analysis. The second line shows the globally adopted error for each observable. That error is multiplied for each observable by a further integer weight factor given in the parenthesis next to the data value. For the data and adopted errors of the neutron-proton Fermi energy differences $\Delta\epsilon_F$ of ^{16}O , ^{40}Ca , ^{48}Ca , ^{56}Ni , ^{132}Sn , and ^{208}Pb as well as the breathing mode energy E_{GMR} of ^{208}Pb , see the text. For the charge-weak form factor difference ΔF_{CW} , the CREX and PREX-2 results, i.e., $\Delta F_{\text{CW}}(q = 0.8733 \text{ fm}^{-1}) = 0.0277 \pm 0.0055$ for ^{48}Ca and $\Delta F_{\text{CW}}(q = 0.3977 \text{ fm}^{-1}) = 0.041 \pm 0.013$ for ^{208}Pb [1], are used in this work.

Nuclei	E_B (1 MeV)	r_c (0.02 fm)	R_d (0.04 fm)	σ (0.04 fm)	$\Delta\epsilon_{ls}$ (20%)
^{16}O	-127.620 (4)	2.701(2)	2.777(2)	0.839(2)	6.30(3) 6.10(3)
^{40}Ca	-342.051 (3)	3.478(1)	3.845(1)	0.978(1)	
^{48}Ca	-415.990 (1)	3.479(2)	3.964(1)	0.881(1)	
^{56}Ni	-483.990 (5)	3.750(9)			
^{68}Ni	-590.430 (1)				
^{100}Sn	-825.800 (2)				
^{132}Sn	-1102.900(1)				1.35(1) 1.65(1)
^{208}Pb	-1636.446(1)	5.504(1)	6.776(1)	0.913(1)	1.32(1) 0.90(1) 1.77(2)

Note: $\Delta\epsilon_{ls}$ data are for $^{16}\text{O}(1p_p, 1p_n)$, $^{132}\text{Sn}(2p_p, 2d_n)$, and $^{208}\text{Pb}(2d_p, 3p_n, 2f_n)$, respectively.

In this work, we also include in our analysis some well-determined data, i.e., the total binding energies E_B , r_c , R_d , σ , spin-orbit splittings $\Delta\epsilon_{ls}$, neutron-proton Fermi energy differences $\Delta\epsilon_F$, and breathing mode energies E_{GMR} of doubly magic nuclei: ^{16}O , ^{40}Ca , ^{48}Ca , ^{56}Ni , ^{68}Ni , ^{100}Sn , ^{132}Sn , ^{208}Pb . The values and adopted errors for E_B , r_c , R_d , σ , and $\Delta\epsilon_{ls}$ are taken from Ref. [36], and listed in Table II for completeness. For $\Delta\epsilon_F$, the experimental values for ^{16}O , ^{40}Ca , ^{48}Ca , ^{56}Ni , ^{132}Sn , and ^{208}Pb are -3.53 , -7.31 , 6.10 , -9.47 , 8.40 , and 0.64 MeV, respectively [37]. According to calculations for $\Delta\epsilon_F$ of 19 nuclei with 54 Skyrme interactions reported in Ref. [37], we take their uncertainties to be 1.2 MeV. As to the E_{GMR} of ^{208}Pb , the weighted average¹ 13.614 ± 0.074 MeV of two independently measured values by RCNP [38,39] and TAMU [40] is used.

IV. RESULTS AND DISCUSSIONS

Bayesian analyses are conducted in four different cases in the present work. The case without including the $\Delta F_{\text{CW}}^{208}$ and $\Delta F_{\text{CW}}^{48}$ is considered as the base point labeled with ‘‘B-Bas’’. The $\Delta F_{\text{CW}}^{48}$ and $\Delta F_{\text{CW}}^{208}$ data are then separately added into the analysis to quantify the tension between the CREX and PREX

¹Here, the weighted average is defined in the standard way, i.e., given n -independent measured value \mathcal{O}_i with the standard deviation σ_i for the same observable, the weighted average is calculated as $\bar{\mathcal{O}} = \frac{\sum_{i=1}^n \mathcal{O}_i / \sigma_i}{\sum_{i=1}^n 1 / \sigma_i}$, and its standard deviation is $\sigma_{\bar{\mathcal{O}}} = (\sum_{i=1}^n \sigma_i^{-2})^{-1/2}$.

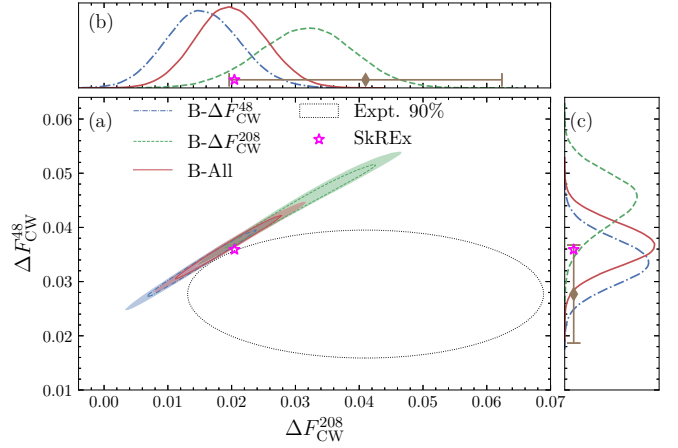


FIG. 1. (a) Joint and (b), (c) marginal distributions of $\Delta F_{\text{CW}}^{208}$ and $\Delta F_{\text{CW}}^{48}$ from B- $\Delta F_{\text{CW}}^{48}$ (blue, dash-dotted line), B- $\Delta F_{\text{CW}}^{208}$ (green, dashed line), and B-All (red, solid line). The shaded regions and the lines correspond to 68.3% and 90% credible regions, respectively. The 90% credible regions of the experimental joint and marginal distributions by CREX and PREX-2 are indicated as the dotted ellipse and solid diamonds, respectively.

data, and the results are accordingly labeled by ‘‘B- $\Delta F_{\text{CW}}^{48}$ ’’ and ‘‘B- $\Delta F_{\text{CW}}^{208}$ ’’. A Bayesian analysis including all the selected observables labeled by ‘‘B-All’’ is further carried out to constrain the $E_{\text{sym}}(\rho)$ by combining the CREX and PREX results. The posterior median values and 68.3% (90%) credible intervals of parameters \mathbf{p} obtained with B-All are listed in Table I.

Figure 1 shows the obtained posterior joint [Fig. 1(a)] and marginal [Figs. 1(b) and 1(c)] distributions of $\Delta F_{\text{CW}}^{208}$ and $\Delta F_{\text{CW}}^{48}$ from B- $\Delta F_{\text{CW}}^{48}$, B- $\Delta F_{\text{CW}}^{208}$, and B-All, together with the corresponding experimental joint distribution of 90% credible region as well as the CREX and PREX individual measurements with 90% uncertainties. It is seen that due to the constraints from properties of doubly magic nuclei, the inferred $\Delta F_{\text{CW}}^{208(48)}$ from B- $\Delta F_{\text{CW}}^{208(48)}$ is less (larger) than the PREX-2 (CREX) measurement. In all the three cases, the inferred 90% confidence regions barely overlap with the experimental one, which indicates the tension between the CREX and PREX-2 results within the framework of Skyrme EDF. From the MCMC samples, we find out a Skyrme interaction (named ‘‘SkREx’’) that is consistent with both the CREX and PREX data at 90% C.L. (as indicated by star in Fig. 1), the measured α_D in ^{48}Ca and ^{208}Pb , and the neutron matter EOS from microscopic calculations as shown later. The parameter values of SkREx are listed in the last column of Table I. The nine Skyrme parameters of SkREx are: $t_0 = -2088.20 \text{ MeV fm}^3$, $x_0 = 0.285971$, $t_1 = 322.498 \text{ MeV fm}^5$, $x_1 = 0.760722$, $t_2 = 537.638 \text{ MeV fm}^5$, $x_2 = -1.66900$, $t_3 = 13965.6 \text{ MeV fm}^{3+3\alpha}$, $x_3 = 0.0165947$, and $\alpha = 0.261515$.

Shown in Fig. 2 are the posterior distributions of $E_{\text{sym}}(2\rho_0/3)$, $L(2\rho_0/3)$, $E_{\text{sym}}(\rho_0)$, and L from the four cases. It is seen from Fig. 2(a) that for B-Bas, the $E_{\text{sym}}(2\rho_0/3)$ has already been well constrained by properties of doubly magic nuclei, and further including ΔF_{CW} has minor effects on the posterior distribution of $E_{\text{sym}}(2\rho_0/3)$. With the $E_{\text{sym}}(2\rho_0/3)$ tightly constrained, the $L(2\rho_0/3)$, $E_{\text{sym}}(\rho_0)$, and L become

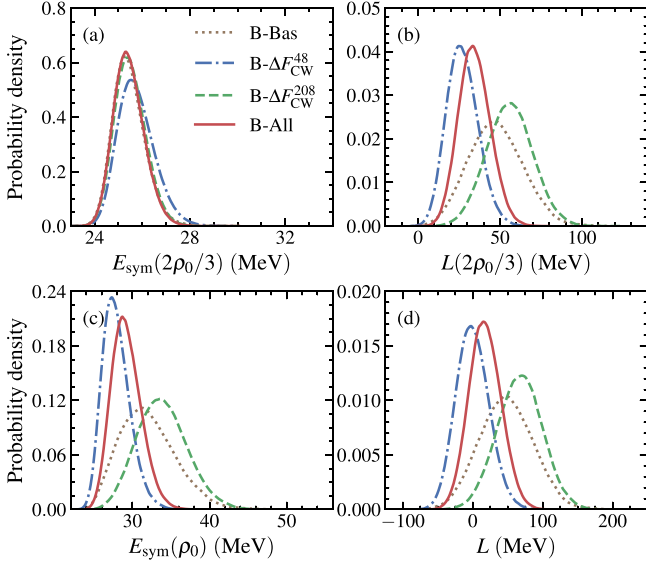


FIG. 2. Posterior distributions of (a) $E_{\text{sym}}(2\rho_0/3)$, (b) $L(2\rho_0/3)$, (c) $E_{\text{sym}}(\rho_0)$, and (d) L in the four cases (see text for details).

highly correlated, leading to very similar shapes for their posterior distributions as shown in Figs. 2(b)–2(d). Unlike the $E_{\text{sym}}(2\rho_0/3)$, the $L(2\rho_0/3)$, $E_{\text{sym}}(\rho_0)$, and L are all weakly constrained with B-Bas, with their posterior distributions exhibiting large distribution widths. Comparing the results from $B-\Delta F_{\text{CW}}^{48}$ and $B-\Delta F_{\text{CW}}^{208}$, one sees the tension between CREX and PREX-2. For example, the measured $\Delta F_{\text{CW}}^{208}$ by PREX-2 favors a larger L [i.e., $68^{+32(52)}_{-33(54)}$ MeV at 68.3%(90%) C.L.], while the $\Delta F_{\text{CW}}^{48}$ by CREX prefers a much smaller L [i.e., $-1^{+24(41)}_{-23(36)}$ at 68.3%(90%) C.L.]. The 68.3% credible intervals obtained from the CREX and PREX data are incompatible, whereas the 90% credible intervals overlap within the region of 14.2 to 40.1 MeV. The overlap region of the L distributions extracted from CREX and PREX-2 amounts for about 23%.

From B-All in Fig. 2, we find $E_{\text{sym}}(2\rho_0/3) = 25.4^{+0.7(1.2)}_{-0.6(0.9)}$ MeV, $L(2\rho_0/3) = 34.1^{+10.1(16.8)}_{-9.2(14.8)}$ MeV, $E_{\text{sym}}(\rho_0) = 29.1^{+2.1(3.6)}_{-1.8(2.7)}$ MeV, and $L = 17.1^{+23.8(39.3)}_{-22.3(36.0)}$ MeV at 68.3%(90%) C.L.. The obtained $E_{\text{sym}}(2\rho_0/3) = 25.4^{+1.2}_{-0.7}$ MeV at 90% C.L. is consistent with $E_{\text{sym}}(2\rho_0/3) \approx 26$ MeV [5] and $E_{\text{sym}}(0.1 \text{ fm}^{-3}) = 25.4 \pm 0.8$ MeV [41] obtained, respectively, from relativistic and nonrelativistic EDFs constrained by nuclear masses, as well as $E_{\text{sym}}(0.11 \text{ fm}^{-3}) = 26.2 \pm 1.0$ MeV extracted from $\Delta\epsilon_F$ in doubly magic nuclei [37] and $E_{\text{sym}}(0.11 \text{ fm}^{-3}) = 26.65 \pm 0.2$ MeV extracted from the binding energy difference of heavy isotope pairs [12]. The inferred $E_{\text{sym}}(\rho_0)$ and L from B-All indicate a soft symmetry energy around ρ_0 but are still consistent with many previous constraints. For example, the upper limit of $L = 40.9$ MeV at 68.3% C.L. agrees with the constraint of $L = 53^{+14}_{-15}$ MeV extracted recently by combining astrophysical data, PREX-2 and chiral effective theory calculations [42]. The inferred soft $E_{\text{sym}}(\rho)$ with $L = 17.1$ MeV also agrees well with the recent constraints from analyzing the α_D in neutron-rich Sn isotopes [43].

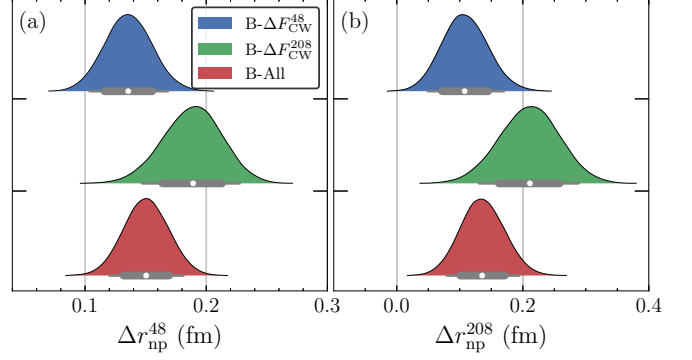


FIG. 3. Posterior distributions of (a) $\Delta r_{\text{np}}^{48}$ and (b) $\Delta r_{\text{np}}^{208}$ for $B-\Delta F_{\text{CW}}^{48}$, $B-\Delta F_{\text{CW}}^{208}$ and B-All. Dots and bars indicate the median values, along with the 68.3% and 90% uncertainties

Shown in Fig. 3 are the posterior distributions of $\Delta r_{\text{np}}^{48}$ and $\Delta r_{\text{np}}^{208}$ for $B-\Delta F_{\text{CW}}^{48}$, $B-\Delta F_{\text{CW}}^{208}$, and B-All. As expected, the CREX (PREX-2) data result in thinner (thicker) Δr_{np} . Again, their 90% credible intervals overlap with each other. The extracted $\Delta r_{\text{np}}^{208} = 0.211^{+0.047}_{-0.049}$ fm (68.3% C.L.) is consistent with 0.283 ± 0.071 fm reported by PREX-2 [2], and the extracted $\Delta r_{\text{np}}^{48} = 0.136^{+0.020}_{-0.020}$ fm (68.3% C.L.) also agrees well with $0.121 \pm 0.026(\text{exp}) \pm 0.024(\text{model})$ fm by CREX [1]. Combining the CREX and PREX data results in $\Delta r_{\text{np}}^{208} = 0.136^{+0.036(0.059)}_{-0.035(0.056)}$ fm and $\Delta r_{\text{np}}^{48} = 0.150^{+0.019(0.031)}_{-0.019(0.030)}$ fm at 68.3% (90%) C.L.. The predicted Δr_{np} is relatively thin, but is still consistent with many previous experimental and theoretical studies [12,26,44], e.g., the very recent *ab initio* predictions of $\Delta r_{\text{np}}^{208} = 0.14 - 0.20$ fm and $\Delta r_{\text{np}}^{48} = 0.14 - 0.19$ fm at 68.3% C.L. [45], and the $\Delta r_{\text{np}}^{48} = 0.15 - 0.21$ fm from $^{54}\text{Ni}-^{54}\text{Fe}$ charge radius difference [46]. Overall, our Bayesian analyses indicate that the CREX and PREX data are compatible with each other at 90% C.L., although they are incompatible at 68.3% C.L.. Furthermore, the inferred results of $E_{\text{sym}}(\rho)$ and Δr_{np} by combining the CREX and PREX data much favor the results from CREX alone, implying the PREX-2 is less effective to constrain the $E_{\text{sym}}(\rho)$ and Δr_{np} due to its lower precision of ΔF_{CW} compared to the CREX.

It is instructive to see the Bayesian inference on the neutron matter EOS $E_{\text{PNM}}(\rho)$, which has been well constrained by microscopic calculations. Figure 4 shows the inferred $E_{\text{PNM}}(\rho)$ by combining the CREX and PREX data at 68.3% and 90% C.L., together with the predictions from many-body perturbation theory using N^3LO chiral interactions by Tews *et al.* [47], Wellenhofer *et al.* [48], and Drischler *et al.* [49], the quantum Monte Carlo methods by Gandolfi *et al.* [50], Wlazłowski *et al.* [51], Roggero *et al.* [52], and Tews *et al.* [53], the variational calculations by Akmal-Pandharipande-Ravenhall (APR) [54], the Bethe-Bruckner-Goldstone calculations (BBG-QM 3h-gap and BBG-QM 3h-con) [55], and the self-consistent Green's function approach (SCGF-N3LO+N2LOdd) [56]. The region indicated by the dash-dot-dotted line in Fig. 4 displays the combined constraint on the $E_{\text{PNM}}(\rho)$ by various microscopic calculations (see also, Ref. [57]). One sees that the inferred $E_{\text{PNM}}(\rho)$ agrees well with the microscopic calculations.

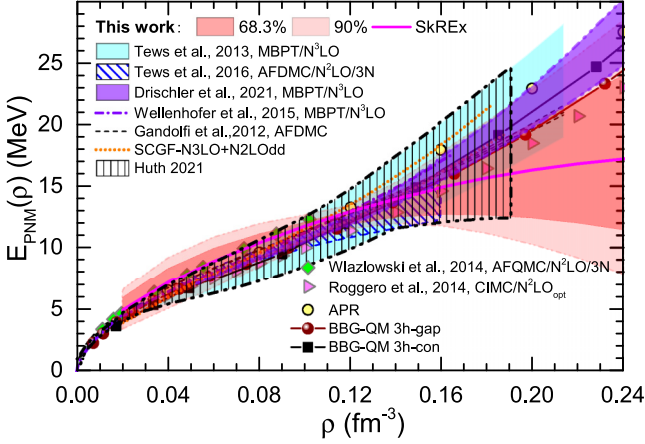


FIG. 4. The Bayesian inferred $E_{\text{PNM}}(\rho)$ by combining CREX and PREX-2 data. The results from microscopic calculations and the Skyrme interaction SkREx are also included for comparison (see text for details).

However, at suprasaturation densities, the inferred $E_{\text{PNM}}(\rho)$ exhibits rather large uncertainties, implying the current data mainly constrain the $E_{\text{PNM}}(\rho)$ at $\rho \lesssim \rho_0$ and more accurate measurements on nuclear weak form factor is necessary to effectively constrain the $E_{\text{PNM}}(\rho)$ at supra-saturation densities.

Figure 5 exhibits the Bayesian inferred binding energy per nucleon in symmetric nuclear matter $E_0(\rho)$ as a function of nucleon density at 90% confidence level by combining CREX and PREX-2 data (B-All, 90%), together with the prediction of the SkREx EDF. For comparison, we also show in Fig. 5 the predictions of chiral effective many-body perturbation theory (χ EMBT) using n3lo414 and n3lo450 forces [48], the 1σ uncertainty band (GP-B) derived from chiral effective theory using a Bayesian approach based on Gaussian process

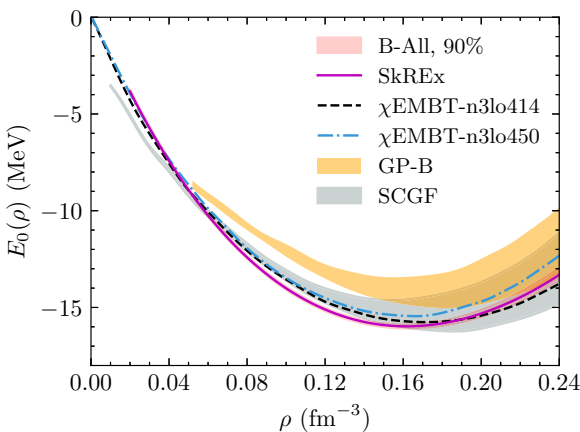


FIG. 5. The Bayesian inferred binding energy per nucleon in symmetric nuclear matter as a function of density ρ at 90% confidence level by combining CREX and PREX-2 data (B-All, 90%), together with the prediction of SkREx EDF. The dashed and dash-dotted lines represent the χ EMBT calculations using n3lo414 and n3lo450 forces, respectively [48]. The orange region displays the 1σ uncertainty band derived from chiral effective theory in Ref. [49], and the gray band is the result of SCGF approach [58].

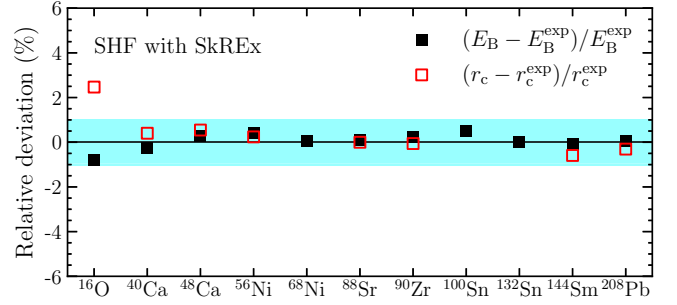


FIG. 6. Relative deviation of the binding energies E_B and charge radii r_c of ^{16}O , ^{40}Ca , ^{48}Ca , ^{56}Ni , ^{68}Ni , ^{88}Sr , ^{90}Zr , ^{100}Sn , ^{132}Sn , ^{144}Sm , and ^{208}Pb obtained using the SkREx EDF from the experimental measurements [36,64–66]. The shaded region indicates $\pm 1\%$ relative deviation.

reported in Ref. [49], and the uncertainty band of SCGF approach due to the use of three different chiral forces [58]. One can see that, within the framework of Skyrme energy density functional, the $E_0(\rho)$ up to $1.5\rho_0$ has been well constrained by the properties of finite nuclei. On the other hand, in microscopic calculations, there are relatively large uncertainties in the predicted $E_0(\rho)$, which arise due to the choice of nuclear forces and many-body methods.

Also included in Fig. 4 is the prediction from SkREx, which well agrees with the microscopic calculations. Furthermore, Fig. 6 compares the total binding energies and charge radii of ^{16}O , ^{40}Ca , ^{48}Ca , ^{56}Ni , ^{68}Ni , ^{88}Sr , ^{90}Zr , ^{100}Sn , ^{132}Sn , ^{144}Sm , and ^{208}Pb from SkREx with the experimental values. It is seen that the SkREx EDF overall well reproduces the experimental data with the relative deviations less than 1%, except for the light nucleus ^{16}O for which the mean-field models are relatively less valid. See Table III for the numeric values of SkREx EDF predictions together with experimental data. We also note the SkREx predicts $\Delta r_{\text{np}}^{48} = 0.152$ fm, $\Delta r_{\text{np}}^{208} = 0.141$ fm, $E_{\text{sym}}(2\rho_0/3) = 25.8$ MeV, and $L(2\rho_0/3) = 34.0$ MeV. In addition, the α_D is known as an

TABLE III. Experimental data [36] and predictions of SkREx energy density functional for the total binding energy E_B and charge radii r_c for several typical spherical nuclei.

Nucleus	E_B (MeV)		r_c (fm)	
	Expt.	SkREx	Expt.	SkREx
^{208}Pb	-1636.446	-1637.174	5.504	5.487
^{144}Sm	-1195.740	-1194.686	4.960	4.931
^{132}Sn	-1102.900	-1103.103	-	4.708
^{100}Sn	-825.800	-829.854	-	4.478
^{90}Zr	-783.893	-785.757	4.269	4.266
^{88}Sr	-768.467	-769.317	4.220	4.220
^{68}Ni	-590.430	-590.746	-	3.889
^{56}Ni	-483.900	-485.981	3.750	3.759
^{48}Ca	-415.990	-417.226	3.479	3.498
^{40}Ca	-342.051	-341.227	3.478	3.492
^{16}O	-127.620	-126.595	2.701	2.768

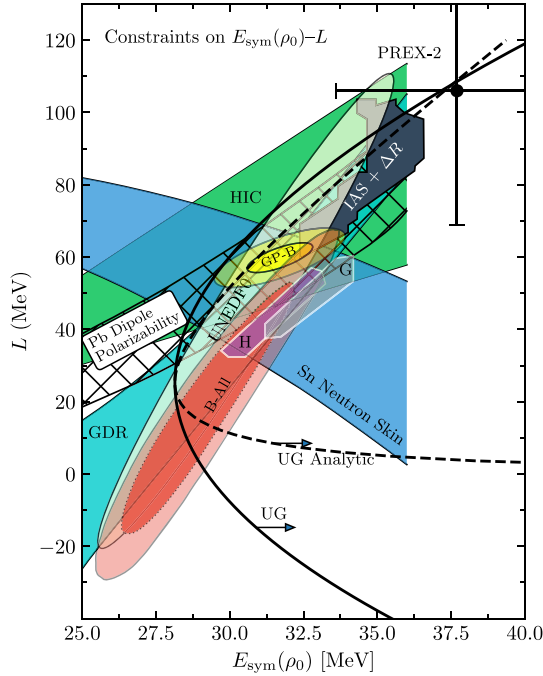


FIG. 7. Constraints on $E_{\text{sym}}(\rho_0)-L$ (see text for details). The 68.3% (90%) region of the posterior joint $E_{\text{sym}}(\rho_0)-L$ distribution inferred with B-All is shown as dark (light-red) area. Adapted from Refs. [18,49].

important isovector indicator [26,44,59–62]. Analyses based on modern nuclear EDFs suggest a strong correlation between $\alpha_D^{208} E_{\text{sym}}(\rho_0)$ and L [26,44] as well as between α_D^{208} and $E_{\text{sym}}(\rho_0/3)$ [61,62]. The α_D in ^{208}Pb and ^{48}Ca have been determined to be $19.6 \pm 0.6 \text{ fm}^3$ [25,26] and $2.07 \pm 0.22 \text{ fm}^3$ [27], respectively, via forward-angle proton elastic scattering experiments. From CHF calculation [63] with SkREx, we obtain $\alpha_D^{48} = 2.24 \text{ fm}^3$ and $\alpha_D^{208} = 19.5 \text{ fm}^3$, agreeing well with the data.

Finally, we plot in Fig. 7 the posterior joint $E_{\text{sym}}(\rho_0)-L$ distribution in the 68.3% and 90% credible regions with B-All. For comparison, we also include the constraints summarized in Refs. [17,18,49], i.e., those from transport model analyses of midperipheral heavy-ion collisions (HIC) [67] and 90% confidence region predicted by UNEDF0 EDF [33], the neutron skin in Sn isotopes [31], the α_D in ^{208}Pb [44], the centroid energy of giant dipole resonance (GDR) in ^{208}Pb [68], the combination of isobaric analog state and isovector skins (IAS+ ΔR) [69], and the neutron skin in ^{208}Pb from PREX-2 [2,17]. Also shown in Fig. 7 are the results from microscopic calculations by Hebeler *et al.* (H) [70], Gandolfi *et al.* (G) [50], and the BUQEYE collaboration (GP-B) [49], as well as from the unitary gas (UG) limit by Tews *et al.* [71]. Overall, the B-All suggests a soft symmetry energy, mainly due to the smaller ΔF_{CW} in ^{48}Ca measured by CREX. A

soft $E_{\text{sym}}(\rho)$ around ρ_0 will have important implications on neutron star properties. For example, a softer $E_{\text{sym}}(\rho)$ around ρ_0 generally gives a higher value of the neutron star core-crust transition density ρ_t [73,74], which plays a critical role in understanding many properties of neutron stars [5,15,75,76]. Using the dynamical method [73], we find that the B-All gives $\rho_t = 0.097^{+0.026(0.049)}_{-0.016(0.023)} \text{ fm}^{-3}$ at 68.3% (90%) C.L., favoring a significantly larger ρ_t value compared to the fiducial $\rho_t = 0.075 \text{ fm}^{-3}$ [77]. In addition, the possible soft $E_{\text{sym}}(\rho)$ at suprasaturation densities inferred in the present work may imply that the quark-hadron phase transition may happen at a relatively low density [78], or the non-Newtonian gravity may be needed to explain the observations of neutron stars [79]. Besides its significance in neutron-star physics, the soft symmetry energy also has important impacts on various issues in nuclear physics studies. Notably, it has considerable effects on the location of neutron-drip line and the astrophysical r-process path [72,80], and the small L value may imply the possible existence of the quasibound state of pure neutron matter [72].

V. CONCLUSIONS

Using Bayesian inference method and the Skyrme EDF, we have demonstrated that the CREX and PREX-2 data are compatible with each other at 90% C.L., although they are incompatible at 68.3% C.L.. We have further obtained a new Skyrme interaction SkREx, which can describe the CREX and PREX-2 data at 90% C.L., the measured α_D in ^{48}Ca and ^{208}Pb , and the microscopic neutron matter EOS. Our Bayesian analyses indicate that the PREX-2 is less effective to constrain the $E_{\text{sym}}(\rho)$ and Δr_{np} due to its lower precision of ΔF_{CW} compared to the CREX, implying the more precise determination of ΔF_{CW} from future MREX experiment [81] or the RES-NOVA experiment via the detection of nearby core-collapse supernova neutrinos [82–84] is of particular importance. Overall, the thinner neutron skin in ^{48}Ca and ^{208}Pb together with a soft $E_{\text{sym}}(\rho)$ around ρ_0 have been inferred from combining the CREX and PREX-2 data, i.e., $\Delta r_{\text{np}}^{208} = 0.136^{+0.036(0.059)}_{-0.035(0.056)} \text{ fm}$, $\Delta r_{\text{np}}^{48} = 0.150^{+0.019(0.031)}_{-0.019(0.030)} \text{ fm}$, $E_{\text{sym}}(\rho_0) = 29.1^{+2.1(3.6)}_{-1.8(2.7)} \text{ MeV}$, and $L = 17.1^{+23.8(39.3)}_{-22.3(36.0)} \text{ MeV}$ at 68.3%(90%) C.L.. The soft $E_{\text{sym}}(\rho)$ around ρ_0 will have important implications on neutron star physics and nuclear physics.

ACKNOWLEDGMENTS

This work was supported in part by the National Natural Science Foundation of China under Grants No. 12235010, No. 11905302, and No. 11625521, the National SKA Program of China No. 2020SKA0120300, and the Fundamental Research Funds for the Central Universities, Sun Yat-Sen University (No. 22qntd1801).

[1] D. Adhikari *et al.* (CREX), *Phys. Rev. Lett.* **129**, 042501 (2022).
 [2] D. Adhikari *et al.* (PREX), *Phys. Rev. Lett.* **126**, 172502 (2021).

[3] B. A. Brown, *Phys. Rev. Lett.* **85**, 5296 (2000).
 [4] S. Typel and B. A. Brown, *Phys. Rev. C* **64**, 027302 (2001).

- [5] C. J. Horowitz and J. Piekarewicz, *Phys. Rev. Lett.* **86**, 5647 (2001).
- [6] R. J. Furnstahl, *Nucl. Phys. A* **706**, 85 (2002).
- [7] L.-W. Chen, C. M. Ko, and B.-A. Li, *Phys. Rev. C* **72**, 064309 (2005).
- [8] M. Centelles, X. Roca-Maza, X. Vinas, and M. Warda, *Phys. Rev. Lett.* **102**, 122502 (2009).
- [9] M. Warda, X. Vinas, X. Roca-Maza, and M. Centelles, *Phys. Rev. C* **80**, 024316 (2009).
- [10] X. Roca-Maza, M. Centelles, X. Vinas, and M. Warda, *Phys. Rev. Lett.* **106**, 252501 (2011).
- [11] B. K. Agrawal, J. N. De, and S. K. Samaddar, *Phys. Rev. Lett.* **109**, 262501 (2012).
- [12] Z. Zhang and L.-W. Chen, *Phys. Lett. B* **726**, 234 (2013).
- [13] V. Baran, M. Colonna, V. Greco, and M. Di Toro, *Phys. Rep.* **410**, 335 (2005).
- [14] A. W. Steiner, M. Prakash, J. M. Lattimer, and P. J. Ellis, *Phys. Rep.* **411**, 325 (2005).
- [15] J. M. Lattimer and M. Prakash, *Phys. Rep.* **442**, 109 (2007).
- [16] B. A. Li, L. W. Chen, and C. M. Ko, *Phys. Rep.* **464**, 113 (2008).
- [17] B. T. Reed, F. J. Fattoyev, C. J. Horowitz, and J. Piekarewicz, *Phys. Rev. Lett.* **126**, 172503 (2021).
- [18] J. M. Lattimer and A. W. Steiner, *Eur. Phys. J. A* **50**, 40 (2014).
- [19] B. A. Li and X. Han, *Phys. Lett. B* **727**, 276 (2013).
- [20] M. Oertel, M. Hempel, T. Klähn, and S. Typel, *Rev. Mod. Phys.* **89**, 015007 (2017).
- [21] T.-G. Yue, L.-W. Chen, Z. Zhang, and Y. Zhou, *Phys. Rev. Res.* **4**, L022054 (2022).
- [22] J. Piekarewicz, *Phys. Rev. C* **104**, 024329 (2021).
- [23] P.-G. Reinhard, X. Roca-Maza, and W. Nazarewicz, *Phys. Rev. Lett.* **127**, 232501 (2021).
- [24] B. Biswas, *Astrophys. J.* **921**, 63 (2021).
- [25] A. Tamii, I. Poltoratska, P. Von Neumann-Cosel, Y. Fujita, T. Adachi, C. A. Bertulani, J. Carter, M. Dozono, H. Fujita, K. Fujita, K. Hatanaka, D. Ishikawa, M. Itoh, T. Kawabata, Y. Kalmykov, A. M. Krumbholz, E. Litvinova, H. Matsubara, K. Nakanishi, R. Neveling *et al.*, *Phys. Rev. Lett.* **107**, 062502 (2011).
- [26] X. Roca-Maza, X. Viñas, M. Centelles, B. K. Agrawal, G. Colo, N. Paar, J. Piekarewicz, and D. Vretenar, *Phys. Rev. C* **92**, 064304 (2015).
- [27] J. Birkhan *et al.*, *Phys. Rev. Lett.* **118**, 252501 (2017).
- [28] P.-G. Reinhard, X. Roca-Maza, and W. Nazarewicz, *Phys. Rev. Lett.* **129**, 232501 (2022).
- [29] E. Yüksel and N. Paar, *Phys. Lett. B* **836**, 137622 (2023).
- [30] U. von Toussaint, *Rev. Mod. Phys.* **83**, 943 (2011).
- [31] L. W. Chen, C. M. Ko, B. A. Li, and J. Xu, *Phys. Rev. C* **82**, 024321 (2010).
- [32] L.-W. Chen and J.-Z. Gu, *J. Phys. G: Nucl. Part. Phys.* **39**, 035104 (2012).
- [33] M. Kortelainen, T. Lesinski, J. Moré, W. Nazarewicz, J. Sarich, N. Schunck, M. V. Stoitsov, and S. Wild, *Phys. Rev. C* **82**, 024313 (2010).
- [34] M. Bender, P.-H. Heenen, and P.-G. Reinhard, *Rev. Mod. Phys.* **75**, 121 (2003).
- [35] J. Friedrich and N. Voegler, *Nucl. Phys. A* **373**, 192 (1982).
- [36] P. Klüpfel, P. G. Reinhard, T. J. Burvenich, and J. A. Maruhn, *Phys. Rev. C* **79**, 034310 (2009).
- [37] N. Wang, L. Ou, and M. Liu, *Phys. Rev. C* **87**, 034327 (2013).
- [38] D. Patel, U. Garg, M. Fujiwara, T. Adachi, H. Akimune, G. Berg, M. Harakeh, M. Itoh, C. Iwamoto, A. Long, J. Matta, T. Murakami, A. Okamoto, K. Sault, R. Talwar, M. Uchida, and M. Yosoi, *Phys. Lett. B* **726**, 178 (2013).
- [39] K. B. Howard *et al.*, *Phys. Lett. B* **807**, 135608 (2020).
- [40] D. H. Youngblood, H. L. Clark, and Y. W. Lui, *Phys. Rev. Lett.* **82**, 691 (1999).
- [41] B. A. Brown, *Phys. Rev. Lett.* **111**, 232502 (2013).
- [42] R. Essick, I. Tews, P. Landry, and A. Schwenk, *Phys. Rev. Lett.* **127**, 192701 (2021).
- [43] Z. Z. Li, Y. F. Niu, and W. H. Long, *Phys. Rev. C* **103**, 064301 (2021).
- [44] X. Roca-Maza, M. Centelles, X. Viñas, M. Brenna, G. Colò, B. K. Agrawal, N. Paar, J. Piekarewicz, and D. Vretenar, *Phys. Rev. C* **88**, 024316 (2013).
- [45] B. Hu *et al.*, *Nature Phys.* **18**, 1196 (2022).
- [46] S. V. Pineda *et al.*, *Phys. Rev. Lett.* **127**, 182503 (2021).
- [47] I. Tews, T. Krüger, K. Hebeler, and A. Schwenk, *Phys. Rev. Lett.* **110**, 032504 (2013).
- [48] C. Wellenhofer, J. W. Holt, and N. Kaiser, *Phys. Rev. C* **92**, 015801 (2015).
- [49] C. Drischler, R. J. Furnstahl, J. A. Melendez, and D. R. Phillips, *Phys. Rev. Lett.* **125**, 202702 (2020).
- [50] S. Gandolfi, J. Carlson, and S. Reddy, *Phys. Rev. C* **85**, 032801(R) (2012).
- [51] G. Wlazłowski, J. W. Holt, S. Moroz, A. Bulgac, and K. J. Roche, *Phys. Rev. Lett.* **113**, 182503 (2014).
- [52] A. Roggero, A. Mukherjee, and F. Pederiva, *Phys. Rev. Lett.* **112**, 221103 (2014).
- [53] I. Tews, S. Gandolfi, A. Gezerlis, and A. Schwenk, *Phys. Rev. C* **93**, 024305 (2016).
- [54] A. Akmal, V. R. Pandharipande, and D. G. Ravenhall, *Phys. Rev. C* **58**, 1804 (1998).
- [55] M. Baldo and K. Fukukawa, *Phys. Rev. Lett.* **113**, 242501 (2014).
- [56] A. Carbone, A. Rios, and A. Polls, *Phys. Rev. C* **90**, 054322 (2014).
- [57] S. Huth, C. Wellenhofer, and A. Schwenk, *Phys. Rev. C* **103**, 025803 (2021).
- [58] J. Xu, A. Carbone, Z. Zhang, and C. M. Ko, *Phys. Rev. C* **100**, 024618 (2019).
- [59] P. G. Reinhard and W. Nazarewicz, *Phys. Rev. C* **81**, 051303(R) (2010).
- [60] J. Piekarewicz, B. K. Agrawal, G. Colo, W. Nazarewicz, N. Paar, P. G. Reinhard, X. Roca-Maza, and D. Vretenar, *Phys. Rev. C* **85**, 041302(R) (2012).
- [61] Z. Zhang and L.-W. Chen, *Phys. Rev. C* **92**, 031301(R) (2015).
- [62] J. Xu, J. Zhou, Z. Zhang, W.-J. Xie, and B.-A. Li, *Phys. Lett. B* **810**, 135820 (2020).
- [63] P. G. Reinhard, B. Schuettrumpf, and J. A. Maruhn, *Comput. Phys. Commun.* **258**, 107603 (2021).
- [64] M. Wang, G. Audi, F. G. Kondev, W. J. Huang, S. Naimi, and X. Xu, *Chin. Phys. C* **41**, 030003 (2017).
- [65] I. Angeli and K. Marinova, *At. Data Nucl. Data Tables* **99**, 69 (2013).
- [66] F. Le Blanc *et al.*, *Phys. Rev. C* **72**, 034305 (2005).
- [67] M. B. Tsang, Y. Zhang, P. Danielewicz, M. Famiano, Z. Li, W. G. Lynch, and A. W. Steiner, *Phys. Rev. Lett.* **102**, 122701 (2009).
- [68] L. Trippa, G. Colo, and E. Vigezzi, *Phys. Rev. C(R)* **77**, 061304 (2008).

- [69] P. Danielewicz, P. Singh, and J. Lee, *Nucl. Phys. A* **958**, 147 (2017).
- [70] K. Hebeler, J. M. Lattimer, C. J. Pethick, and A. Schwenk, *Phys. Rev. Lett.* **105**, 161102 (2010).
- [71] I. Tews, J. M. Lattimer, A. Ohnishi, and E. E. Kolomeitsev, *Astrophys. J.* **848**, 105 (2017).
- [72] K. Oyamatsu, H. Sotani, and K. Iida, *PoS INPC2016*, 136 (2017).
- [73] J. Xu, L.-W. Chen, B.-A. Li, and H.-R. Ma, *Astrophys. J.* **697**, 1549 (2009).
- [74] C. Ducoin, J. Margueron, and C. Providencia, *Europhys. Lett.* **91**, 32001 (2010).
- [75] C. J. Pethick and D. G. Ravenhall, *Annu. Rev. Nucl. Part. Sci.* **45**, 429 (1995).
- [76] K. Oyamatsu and K. Iida, *Phys. Rev. C* **75**, 015801 (2007).
- [77] B. Link, R. I. Epstein, and J. M. Lattimer, *Phys. Rev. Lett.* **83**, 3362 (1999).
- [78] N.-B. Zhang and B.-A. Li, *Eur. Phys. J. A* **59**, 1 (2022).
- [79] D.-H. Wen, B.-A. Li, and L.-W. Chen, *Phys. Rev. Lett.* **103**, 211102 (2009).
- [80] R. Wang and L.-W. Chen, *Phys. Rev. C* **92**, 031303(R) (2015).
- [81] D. Becker *et al.*, *Eur. Phys. J. A* **54**, 208 (2018).
- [82] L. Pattavina, N. Ferreira Iachellini, and I. Tamborra, *Phys. Rev. D* **102**, 063001 (2020).
- [83] L. Pattavina *et al.* (RES-NOVA), *J. Cosmol. Astropart. Phys.* **10**, 064 (2021).
- [84] X.-R. Huang and L.-W. Chen, *Phys. Rev. D* **106**, 123034 (2022).